

Article citation info:

Ma D, Zeng Q, Meng Z, Cheng W, Meshing properties of shearer traction wheel affected with axial sliding, *Eksploracja i Niezawodność – Maintenance and Reliability* 2026; 28(2) <http://10.17531/ein/210715>

## Meshing properties of shearer traction wheel affected with axial sliding

Indexed by:



Dejian Ma<sup>a,b,c</sup>, Qingliang Zeng<sup>b,c</sup>, Zhaosheng Meng<sup>d,c</sup>, Weimin Cheng<sup>a,\*</sup>

<sup>a</sup> College of Safety and Environmental Engineering, Shandong University of Science and Technology, China

<sup>b</sup> College of Mechanical and Electronic Engineering, Shandong University of Science and Technology, China

<sup>c</sup> Shandong Province Key Laboratory of Intelligent Mine Equipment Collaborative Mining Technology, China

<sup>d</sup> State Key Laboratory of Mining Disaster Prevention and Control Cofounded by Shandong Province and the Ministry of Science and Technology, Shandong University of Science and Technology, China

### Highlights


- A meshing model of the traction wheel with axial sliding is established.
- The axial sliding mainly occurs during the alternating meshing of multi-tooth.
- The axial sliding inhibits the eccentric load but aggravates the fatigue wear.
- The load, speed and meshing error angle intensify axial sliding damage.
- The axial driving force decreases the fatigue strength near the tooth root.

### Abstract

Coal mining is an important guarantee for energy supply. But due to the poor spatial stability of the shearer, the collision of traction units is significant. The failure of the traction wheel becomes an important factor restricting the efficiency of coal mining. It is an important scientific problem to explore the failure law of the traction wheels affected with axial slip friction. Therefore, the meshing model of the traction wheel with axial sliding is established. The destructiveness and response properties of axial sliding are analyzed, and the influence of sliding position and axial force is discussed. The results show that the axial fretting sliding reduces the impact contact force on the tooth profile by 50%, but a stress increase of 52 MPa on the tooth surface near the tooth root. The damage on the tooth surface intensifies while the risks of adhesion wear and gluing failure increase, as the increase of load, velocity and meshing error angle. The axial force is more likely to induce forced sliding in the root area. And with the axial driving increase, the forced sliding and its destructiveness aggravate. The results have reference to analyzing meshing properties of traction wheels affected by axial sliding and reducing the shearers' traction failure.

### Keywords

mining equipment. coal and shearer, rolling-sliding contact, failure analysis

This is an open access article under the CC BY license (<https://creativecommons.org/licenses/by/4.0/>) 

### 1. Introduction

Coal production is closely related to world energy security [1]. And because of the advantage of strong bearing capacity, the double drum shearer in modern underground coal mining mainly adopts chainless haulage systems of meshing type [2]. The meshing of the pin tracks and traction wheels is a common transmission method. Its meshing reliability is a pivotal factor affecting the shearer's performance and restricting the

efficiency of coal mines. However, the working condition of the traction wheel is harsh, and it has the characteristics of abrasive pollution, load impact and dry friction [3]. This leads to serious wear and short useful life of traction wheels [4]. Besides, the special structure with double drive on the single side determines the poor spatial pose stability of the shearer [5, 6], which leads to the shearer's runout and shimmy and aggravates the contact

(\*) Corresponding author.

E-mail addresses:

D. Ma (ORCID:0000-0002-6790-4640) [dejian\\_ma@sdust.edu.cn](mailto:dejian_ma@sdust.edu.cn), Q. Zeng (ORCID: 0000-0002-3842-9107) [qlzeng@sdust.edu.cn](mailto:qlzeng@sdust.edu.cn), Z. Meng (ORCID:0000-0002-8103-694X) [skdmzs@163.com](mailto:skdmzs@163.com), W. Cheng (ORCID:0000-0002-9199-288X) [wmsdust@163.com](mailto:wmsdust@163.com)

impact of the wheel. However, the torsional sliding impact contact mechanism and the failure law of the traction wheel are still not completely clear. This makes the traction failure become an important cause of shearer shutdown and restricting the mining efficiency. Therefore, overcoming the frequent failure of traction units and reducing traction failures have become urgent problems for coal equipment.

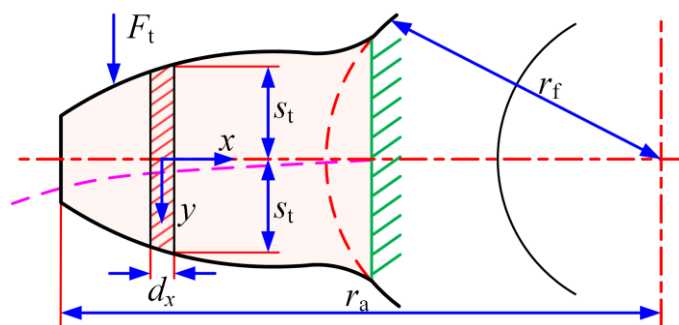
Scholars have studied the shearer traction properties with the help of multi-body dynamics theory and the finite element method. Liu et al. [7, 8] established the torsional dynamic model of the shearer transmission system emphasizing that the meshing stiffness is the key to the system disturbance. Lao et al. [9] realizes the optimal coal loading efficiency of thin seam shearer through collaborative optimization of traction speed and drum speed.. Yang et al. [10] considered the contact gap and analyzed the traction vibration under the condition of oblique cutting. Cheng et al. [11] deduced the tooth profile equation of tooth-pin meshing which have a reference to the traction fault analysis. A modular haulage mechanism was reported in Poland that had advantages in restraining the side clearance and reducing stress damage [12, 13].

Equipment failure is the key factor threatening the safety production[14, 15], and the meshing failure is the main cause of shearer traction failure [16]. Ruihua et al. [17] found that the size of pitting corrosion is an important reason for affecting the meshing stiffness. The root crack reduces the meshing stiffness [18]. Dogan et al. [19] suppressed the root crack propagation by optimizing the hub thickness and pressure angle, which prolonged the useful life by about 15 times. Compared with the traditional prediction model, the bending fatigue life of gears reduces by 22% after considering the adjacent tooth effect [20, 21]. Considering the material hardness and based on the Archard model, Chen et al. [22] established a wear evaluation model of the meshing with the rack and gear. Combined with the discrete element method, Akbar et al. pointed out that the vibration frequency increases the wear coefficient [23], and the wear rate has a power function relationship with the impact speed [24]. Dimaki et al. [25] found that the adhesion force and plastic hardening coefficient determine the wear state, abrasive hardness is the main reason affecting material wear resistance[26]. Zhiying et al. [27] proposed an improved gear load distribution model, which can effectively predict the gear

wear depth combined with the potential energy method. Haibo et al. [28] found that wear accumulation worsens the load distribution in the tooth alternating phase.

The shearer attitude disturbance leads to the torsional and micro motion contact error of the traction wheel [29–31]. And relative sliding and vibration are the key factors to reduce the gear life [32], and sliding friction increase meshing error[33]. Yujing et al. [34] analyzed the influence of contact deformation and backlash on the vibration of bevel gears, and Zhao et al. [35, 36] pointed out that the geometric eccentricity would cause the torsional deformation of gear, which is an important reason for the tooth eccentric load [37]. Wan et al. [38] reported that the shaft misalignment angle would increase the risk of tooth root fracture. Dong et al. [39] proposed an angular velocity analysis model with 6 degrees of freedom of the end gear transmission system. Lu et al. [40] analyzed the combined deformation with bending and torsion of bevel gears and found the torsional deformation at the end of the tooth width was significant.

In conclusion, scholars have conducted considerable research on the shearer traction dynamics and gear meshing failure. However, different from the gear, the traction wheel has complex torsion and sliding in the meshing process, as is shown in 0. The asymmetric spatial structure and time-varying load excitation determine that it is difficult for the shearer to maintain the spatial mechanical balance (as shown in Fig. 1 (a) and (b)), resulting in the spatial swings and relative runout of the traction department (as shown in Fig. 1 (c)). Affected by the shearer's attitude disturbance, the behavior of tooth surface sliding and tooth misalignment appears (as shown in Fig. 1 (d)). Although the existing research involves the shaft misalignment and relative sliding speed  $\Delta v$  of the traction wheel [41], the damaging effect of axial sliding  $\Delta v_z$  is rarely considered. At present, the axial sliding response law and meshing mechanism of the traction wheel are not completely clear, and the damage law of the walking wheel cannot be fully revealed. It means the existing methods cannot solve the axial sliding and meshing failure of traction wheel under complex attitude disturbance. Therefore, the innovation of this paper is to establish a meshing contact model of the traction wheels containing axial sliding, reveal the destructiveness of axial sliding, clarify the sliding responses for traction load, speed and meshing angle error. This research has references to revealing the fault laws of the traction



boundary conditions can be obtained:

$$F_t = -2 \int_{-s_t}^{+s_t} \tau_{xy} b_t dy \quad (7)$$

Due to the zero load on both ends of the tooth body, the boundary conditions can be obtained:

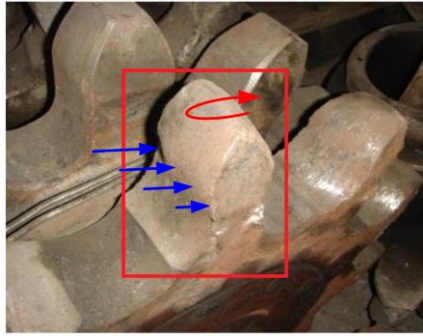
$$\sigma_x = 0 \quad (x = 0) \quad (8)$$

$$\sigma_y = \tau_{xy} = 0 \quad (y = \pm s_t) \quad (9)$$

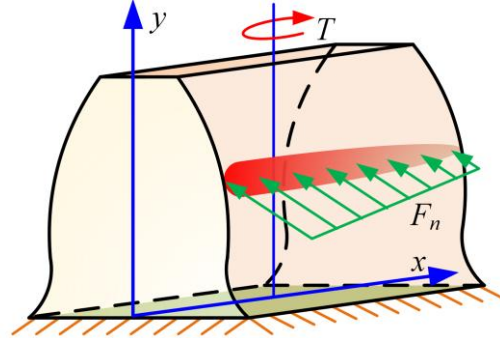
According to the inverse solution of the stress function, the stress state of the tooth body during bending deformation can be obtained:

$$\begin{cases} \sigma_x = -\frac{3F_t xy}{4b_t s_t^3} = -\frac{F_t xy}{J_x} \\ \sigma_y = 0 \\ \tau_{xy} = -\frac{3F_t}{8b_t s_t^3} (s_t^2 - y^2) = -\frac{F_t}{2J_x} (s_t^2 - y^2) \end{cases} \quad (10)$$

where  $J_x = 4b_t s_t^3/3$  is the inertial distance with the x-axis of the longitudinal section of the column.



(a)



(b)

Fig. 3. The tooth torsional deformation of the walking wheel: (a) plastic torsion deformation failure of the tooth; (b) tooth torsion model.

And there is a stress function  $\vartheta(x, y)$ :

$$\frac{\partial^2 \vartheta(x, y)}{\partial y^2} - \frac{\partial^2 \vartheta(x, y)}{\partial x^2} = -2G\theta_{td} \quad (13)$$

The boundary value of the stress function on the tooth surface is:

$$\vartheta(x, y) = 0 \quad (|x| = b_t, \quad |y| = s_t) \quad (14)$$

The stress function is obtained according to Poisson's equation and boundary conditions:

$$\vartheta = -G\theta_{td} \left[ y^2 - s_t^2 + \frac{32s_t^2}{\pi^3} \sum_{n=1,3,5,\dots}^{\infty} \cos \frac{n\pi y}{2s_t} \frac{\sin(\frac{n\pi}{2})}{n^3 \cosh(\frac{n\pi b_t}{2s_t})} \cosh \frac{n\pi x}{2s_t} \right] \quad (15)$$

The torque  $M_{td}$  of the tooth body is obtained after the surface

integral of  $\vartheta(x, y)$ :

$$M_{td} = 2 \iint \vartheta dx dy = 16G\theta_{td} b_t s_t^3 \left[ \frac{1}{3} - \frac{64s_t}{b_t \pi^5} \sum_{n=1,3,5,\dots}^{\infty} \frac{\tanh(\frac{n\pi b_t}{2s_t})}{n^5} \right] \quad (16)$$

The shear stress of the tooth body is obtained according to

the stress function  $\vartheta(x, y)$ :

However, under the influence of the shearer's attitude disturbance, the axial sliding  $\Delta v_z$  occurs and the meshing force on the tooth surface is no longer axial uniformly distributed, as shown in 0(c) and (d). The tooth body undergoes plastic torsional deformation failure under the axial unbalanced load, as shown in 0(a). The torsional angle of the tooth body is assumed to be  $\theta_{td}$ , as shown in 0(b). Ignoring the warping caused by the constraint torsion of the column with a variable cross-section, the elasticity basic equation can be simplified as:

$$\begin{cases} \frac{\partial \tau_{zx}}{\partial z} = 0 \\ \frac{\partial \tau_{zy}}{\partial z} = 0 \\ \frac{\partial \tau_{zx}}{\partial x} + \frac{\partial \tau_{zy}}{\partial y} = 0 \end{cases} \quad (11)$$

$$\frac{\partial \tau_{zx}}{\partial y} - \frac{\partial \tau_{zy}}{\partial x} = -2G\theta_{td} \quad (12)$$

where,  $G$  is shear modulus.

$$\begin{cases} \tau_{zx} = -\frac{M_{td}}{16\alpha_{td}b_t s_t^3} \left[ 2y - \frac{16s_t}{\pi^2} \sum_{1,3,5,\dots}^{\infty} \frac{\sin(\frac{n\pi}{2})}{n^3 \cosh(\frac{n\pi b_t}{2s_t})} \cosh \frac{n\pi x}{2s_t} \sin \frac{n\pi y}{2s_t} \right] \\ \tau_{zy} = \frac{M_{td}}{\alpha_{td}b_t s_t^2} \sum_{1,3,5,\dots}^{\infty} \frac{\sin(\frac{n\pi}{2})}{n^3 \cosh(\frac{n\pi b_t}{2s_t})} \cos \frac{n\pi y}{2s_t} \sinh \frac{n\pi x}{2s_t} \end{cases} \quad (17)$$

## 2.2. System modeling and simulation

As shown in 0, the meshing contact model of single pin track and involute traction wheel is established [43–45]. And the modeling process is shown in 0 (b). The mesh generation of the finite element model is completed in the software of HyperMesh. The finite element is the hexahedron type. The material properties of the traction wheels and the pin tracks are shown in Table 1. The pre-processing of the simulation is completed in the software of LS-PrePost. The drive input is simplified, and

the angular velocity is adopted as the drive of the traction wheel. The angular velocity is converted according to the translation of the pin track where the pin pitch is 147 mm and the traction wheel has 11 teeth:

$$\omega = \frac{\pi v}{30Pz} \quad (18)$$

where  $\omega$  is the angular velocity;  $v$  is the shearer's traction velocity;  $P$  is the pin track's pitch;  $z$  is the number of teeth of the traction wheel.

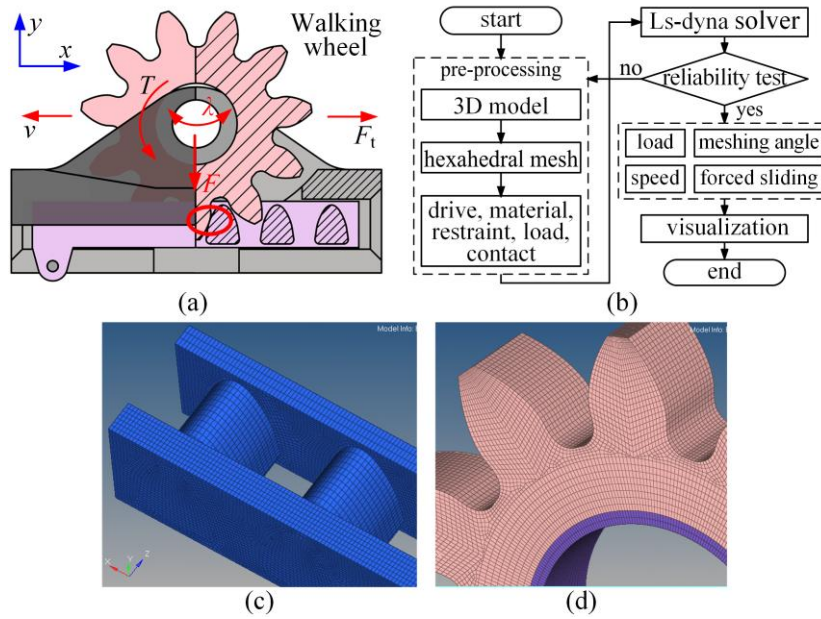


Fig. 4. The model of the simulation: (a) the simulation model of the traction wheel meshing; (b) the flowchart of the simulation; (c) the finite element mesh of the pin track; (d) the finite element mesh of the traction wheel.

The degree of freedom of the pin track is set equivalently and the movement of the pin tracks is unconstrained along the x-axis. The traction load of the wheel is set as 120 kN and the support load is set as 100 kN. In the simulation model, the free torsion of the traction wheel is constrained, and the rolling angle and oblique angle are set quantitatively during meshing. To simulate the axial free sliding state of the traction wheel, the translational constraint of the traction wheel in the axle direction is released. The axial driving force is set to simulate the axial forced sliding of the traction wheel under the disturbance of the

shearer's attitude and cutting force. The contact between the pin tracks and traction wheels is defined by the penalty function. The finite element model is solved by the software of the ANSYS/LS-DYNA display solver. To improve the accuracy of the solution, the mesh of the contact area of the traction wheel is refined. After the mesh independence test, the number of meshes is finally determined to be 295997 [45], and the meshing contact force on the tooth surface tends to be stable.

As an example to test the simulation model, the tooth stress distribution is obtained in 0 (a) and (b), with the traction speed



of 0.2 m/s. The result shows that the tooth stress laws is supported by the result of the figure 4(b) of Chen [46] and the figure 12(a) in the literature of Hu [47], and basically conforms

Table 1. Material properties of the pin track and traction wheel.

Part name	Materials	Elastic modulus	Density	Poisson ratio
Traction wheel	18Cr2Ni4WA	$2.02 \times 10^{11}$ Pa	7900 kg/m <sup>3</sup>	0.27
Pin track	40CrMnMo	$2.06 \times 10^{11}$ Pa	7910 kg/m <sup>3</sup>	0.3

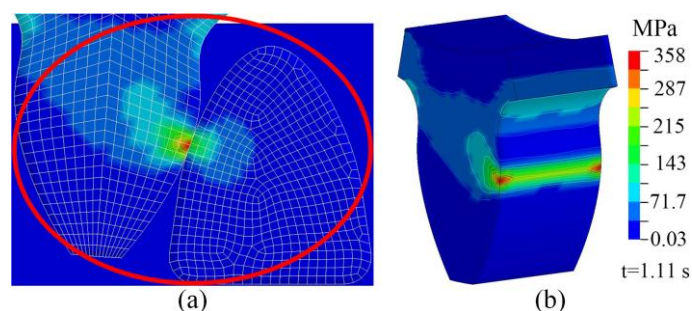


Fig. 5. The stress distribution in the simulation: (a) on the end face of the tooth; (b) on the tooth surface.

### 2.3. Shearer traction experiment and traction wheel swing test

To analyze the axial slip of the traveling wheel and check the model reliability, a traction test bench is built according to the similarity principle[48], as shown in 0. The simulation model will be verified by the contrastive analysis of the axial motion of the walking wheel in the experiment and simulation. Affected by the actual direction and the connection gap of the scraper conveyor, the real-time relative displacement between the shearer and the scraper conveyor is difficult to measure directly.

to the traction wheel's actual wear [45]. This indicates that the simulation model has a certain degree of credibility.

But, the angular velocity of the traction wheel around the x and y axes can indirectly reflect its axial slip characteristics relative to the pin teeth, since the rotation of the shearer around the x and y axes is the decisive factor of the axial slip, as illustrated by 0. Therefore, the coincidence between the axial slip analysis in the simulation and the angular velocity characteristics in the experiment will be the basis for verifying the existence of axial slip and the feasibility of the simulation model.

The test model is designed according to the shearer of MG650/1620-WD with a similarity ratio of 1:5. The center distance of the traction wheels of the shearer for the test is 1270 mm, the length of the cutting arm is 548 mm, the width of the body is 320 mm, and the height of the body is 310 mm. The experiment principle is shown in 0(b), the sensors interact with Bluetooth HID (human interface device) hosts through feature report protocol, and the upper computer connects with HID hosts through the USB interface to achieve signal display, acquisition, and sensor control. To facilitate the installation of sensors and signal acquisition, wireless sensors are separately installed at the axle ends of two traction wheels as shown in 0(a).



Fig. 6. Shearer traction experiment and its principle: (a) shearer traction experiment system; (b) the experiment principle.

The BWT61CL multifunctional vibration sensor is selected,

which can simultaneously test acceleration, angular velocity

and attitude angle signals of the x, y and z axis and transmit wirelessly through Bluetooth. The sensor is installed with a vertical pattern, with the x-axis pointing to the traction direction of the shearer, the y-axis pointing to the vertical direction, and the z-axis pointing to the goaf along the walking wheel axis. The acceleration and attitude of the sensor are calibrated concerning the initial position of the shearer. The maximum hauling stroke of the shearer is 2.5m, which is within the use range of the maximum transmission distance of sensors of 10 m.

### 3. Results and discussion

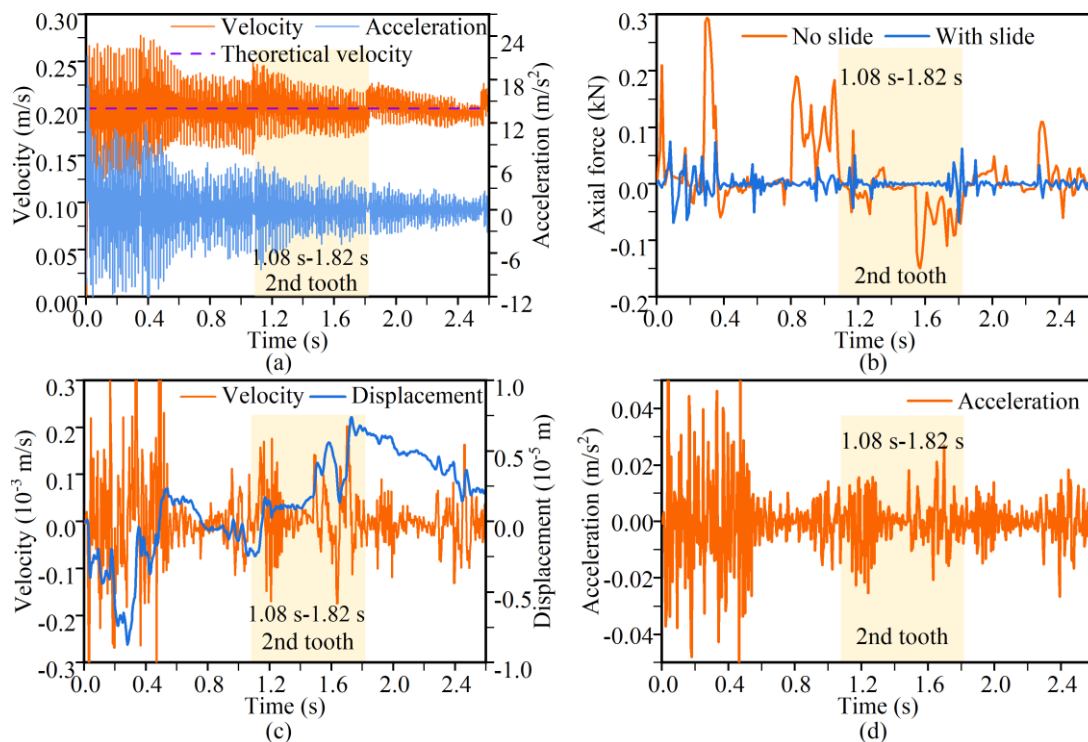


Fig. 7. The motion characteristics of the traction and axial sliding of the traction wheel: (a) traction speed and acceleration; (b) the axial contact force; (c) the axial sliding velocity and displacement; (d) the axial sliding acceleration.

As shown in 0(a), with the simulation entering the stable stage, the average speed gradually converges to 0.2 m/s. This indicates that the simulated result of the traction velocity is basically in agreement with the theoretical value of 0.2 m/s. And the results show that the axial sliding disturbance does not significantly reduce the shearer's hauling velocity.

0(b) is the difference in the axial force under the influence of axial sliding of the traction wheel. The result shows that the second tooth participates in complete meshing between 1.08 s and 1.82 s. Under the axial constraint state, the axial force has a significant periodicity. The maximum axial force of the traction

#### 3.1. Analysis of axial sliding characteristics of the traction wheel

The relative sliding friction behavior under high load is a critical factor to affect the traction wheel's wear failure[45, 49]. Therefore, to research the contact response and the axial sliding law of the traction wheel, the axial motion constraint is adjusted to simulate the axial sliding disturbance of the traction wheel. The hauling velocity is defined as 0.2 m/s and the traction load is defined as 120 kN. And the traction motion and axial sliding motion characteristics within 2.6 s are obtained. and the differences in the axial contact force and equivalent stress distribution of the tooth surface are compared.

wheel is 0.184 kN when a single tooth meshes in, and 0.149 kN when the meshing out. The axial force fluctuated significantly in the multi-tooth alternating meshing stage. The force direction was positive at the meshing-in time and negative at the meshing-out time, but the force direction does not change significantly at the same meshing time. Besides, the axial force and its fluctuation duration decrease relatively in the axial sliding state. The maximum axial force decreases by 72% to 0.051 kN at the meshing-in time and decreases by 54% to 0.068 kN at the meshing-out time. This is because the axial friction changes from static friction to dynamic friction affected by the

tooth sliding, and the dynamic friction decreases relative to the static friction. And the axial sliding inhibits the collision contact on the tooth profile which reduces the axial component of the meshing force. The difference from the axial constraint state is that the axial force direction changes repeatedly at the same meshing time under the axial constraint state. This is because the axial reciprocating sliding causes repeated changes in the axial friction direction. The result indicates that axial sliding will suppress the axial force of the traction wheel, which contributes to weakening the impact on the wheel profile.

As shown in 0(c) and 0(d), the axial acceleration, velocity and displacement of the traction wheel are got respectively. The result shows that the traction wheel slides in the positive direction as a whole during the second tooth meshing, and the maximum sliding distance is  $9.84 \times 10^{-4}$  m. The axial velocity

and acceleration fluctuate violently at the meshing-in and meshing-out time, which indicates that the axial sliding is intensified while the multi-tooth alternating meshing. However, the axial speed decreases with the axial sliding weakening, in the middle time of a tooth meshing. This is related to the increase in axial force and the collision intensification of the tooth surface under the influence of the meshing impact during the multi-tooth alternating. Besides, the meshing of the traction wheel is mainly rolling contact, but the axial friction on the tooth is generated caused by the axial sliding. And the normal force on the meshing face increases with the increase in the traction load, which leads to an increase in axial friction. Therefore, although axial sliding suppresses axial collision contact on the tooth profile, it worsens the tooth surface wear.

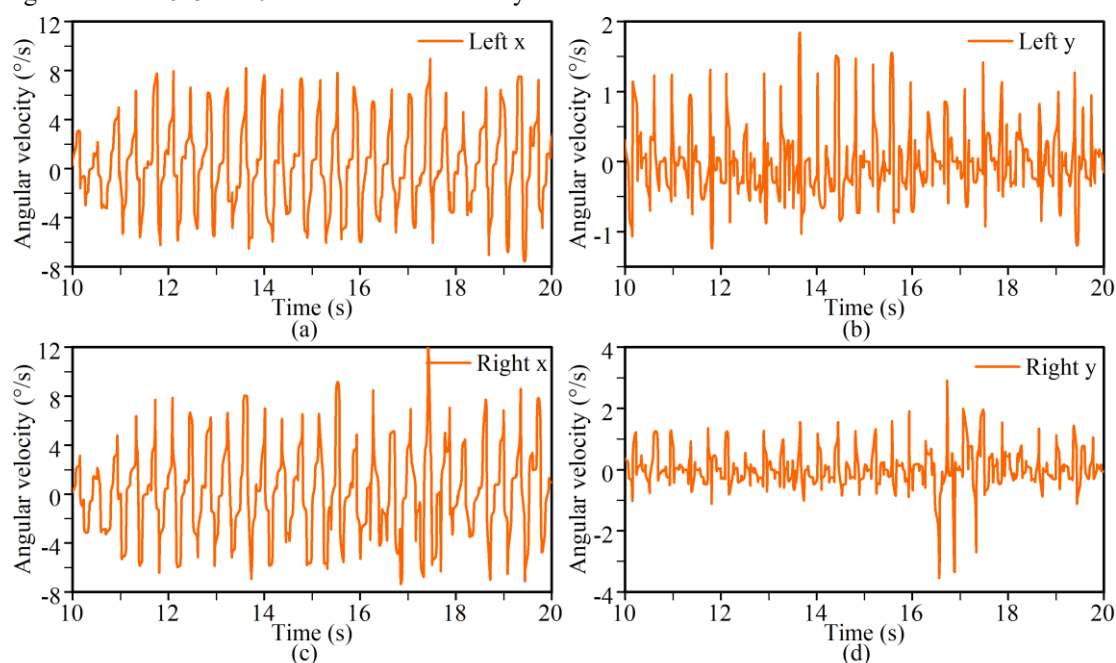


Fig. 8. Angular velocity of the traction wheels obtained from the experiment: (a) the left traction wheel around the x-direction; (b) the left traction wheel around the y-direction; (c) the right traction wheel around the x-direction; (d) the right traction wheel around the y-direction.

To verify the model reliability and the analysis results, the no-load traction of the shearer was carried out on the experimental platform of the fully mechanized mining face. As shown in 0(c), the main reason that affects the axial sliding is that the traction wheel rotates in the x and y directions. Therefore, only the angular velocities of the left and right traction wheels in the x and y directions are obtained, as shown in 0. The test results show that the traction wheel has

reciprocating rotation around the x and y directions. The right traction wheel swings more violently than the left, and the effective values of the angular velocity of the left traction wheel are 3.30 °/s and 0.47 °/s while 3.51 °/s and 0.64 °/s of the right. This may be because the overall attitude disturbance causes more severe torsion of the right traction unit. The experiment data support the simulation results and analysis in 0 (c). The rotation on the end of the traction wheel shaft around the x and



y axes provides an experimental basis for the existence of axial sliding friction during the meshing between the tooth and pin track. This reflects the simulation model reliability. Besides, the periodic effect of the meshing on axial sliding is relatively weak in the experimental results. This shows that the connection clearance of the scraper conveyor may be another important factor affecting the axial sliding, except for the multi-tooth alternate meshing. And the axial sliding of traction wheels in the actual traction is worse than that in the simulated conditions. This also reflects that the influence of axial sliding on the traction wheel meshing cannot be ignored.

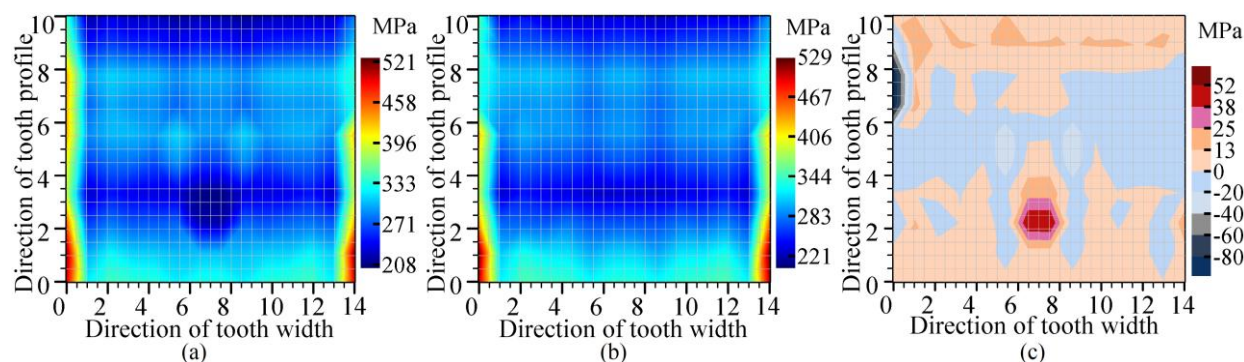


Fig. 9. The maximum stress distribution in a single meshing period: (a) without the axial sliding; (b) with the axial sliding; (c) the stress variation amplitude.

The results show that the dangerous areas of the traction wheel are mainly located on the tooth profile affected by the edge effect. Especially the stress concentration near the root is pronounced. This corresponds to the actual condition of serious tooth profile wear in the actual use of the traction wheel and is basically consistent with the analysis result of the literature [50]. The maximum stress on the tooth face is 521 MPa without axial sliding, while 529 MPa with axial sliding friction. The stress overall increase on the tooth root and tooth top is about 20 MPa, and the maximum increase is 52 MPa near the middle region around the tooth root. Without the axial sliding, the initial bending stress is relatively small near the middle area around the tooth root, because the bending deformation on the tooth profiles is more serious than in other positions on the same meshing line under the compression. Although the stress in the middle region increases significantly, its failure effect is weak due to the improvement of the axial stress distribution. Combining the discussion of 0, the stress increase is due to the intensification of the axial reciprocating sliding and axial force fluctuation in the meshing area of the tooth root and tooth top, which leads to the shear stress on the tooth surface increase.

To explore the effect on the traction wheel's damage by the axial sliding, the maximum stress distribution affected by the friction behavior is obtained in the second tooth contact period, as indicated by 0. The tooth surface is divided into 14 equal parts along the direction of the tooth width and 10 equal parts along the direction from the tooth root to the tooth top. The maximum value of any element from 1.08 s to 1.82 s is obtained as the equivalent stress of this area at the contact time, and the load variation on the tooth under the influence of axial sliding is analyzed through the stress difference.

According to the Archard model, the wear depth is positively correlated with the relative sliding rate and contact stress of the contact surface [51], and Wang et al. [52] experimentally verified that the tooth wear increases as the frequency increase of the friction under the dry friction conditions. Therefore, affected by the axial friction, the wear near the tooth root and tip increases in a single meshing period.

In addition, the stress concentration area of the tooth top profile is reduced, and the axial stress distribution is improved. The result indicates that the axial clearance can alleviate the unbalance loading near tooth top and weaken the destruction by torsional deformation to the tooth. Besides, the tooth stress on the area near the pitch line and the middle tooth profile is reduced by about 20 MPa as a whole. This is because the axial sliding on the area near pitch circle slows down, and the tooth profile extrusion weakens under the influence of the axial fretting clearance. This leads to the reduction of meshing impact and equivalent stress in the middle time of a single tooth meshing cycle.

### 3.2. Analysis of the axial sliding response of the traction wheel under different influence

To research generation mechanisms and the wear laws of axial sliding behavior of the traction wheels, as shown in 0 and 0, the

effects of traction load, speed, rolling angle and oblique angle on the axial force and axial sliding speed are analyzed respectively.

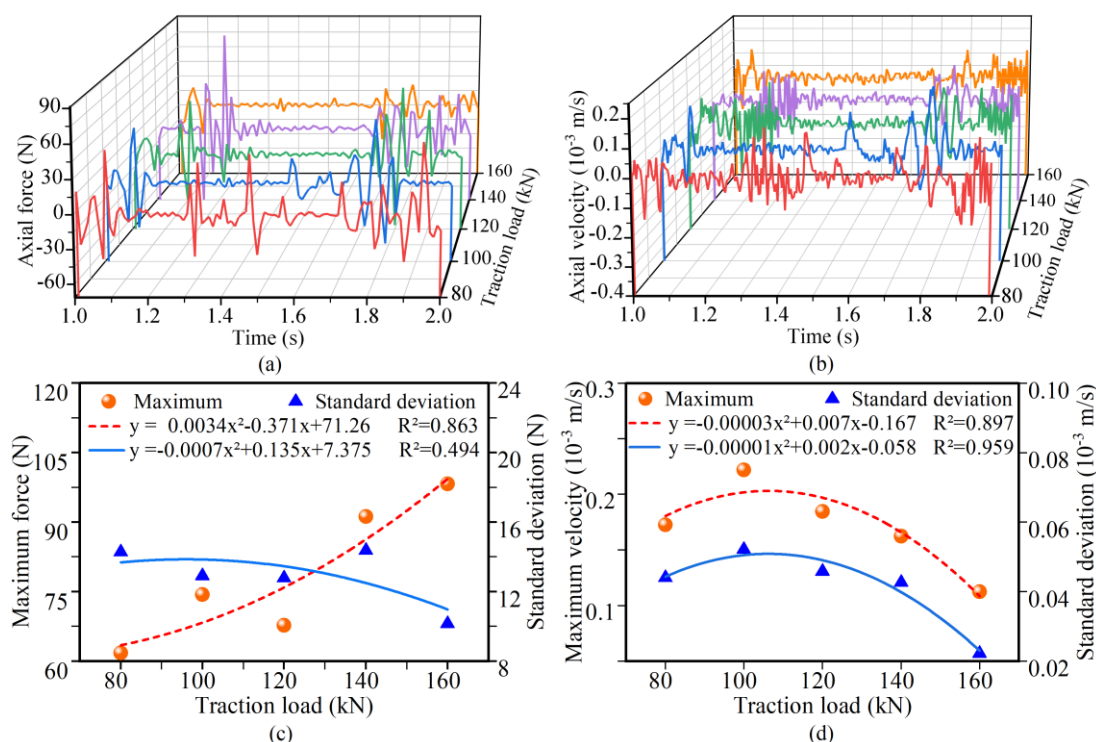


Fig. 10. Axial sliding response of the traction wheel under the influence of traction load: (a) axial force; (b) axial velocity; (c) maximum axial force and its variance; (d) maximum axial velocity and its variance.

To study the effect of traction load, the velocity is set as 0.2 m/s, the traction load is set from 80 kN to 160 kN. The axial sliding speed and axial force are obtained during the stable meshing, respectively. And the maximum value and variance in a complete meshing period are analyzed on the second tooth, as shown in 0. The result shows that the maximum axial force increases by 35% to 98 N but the variances of the axial force decrease slightly, with the increase of the traction load of the shearer. The axial force fluctuation is significant while the tooth alternates meshing, but the axial force fluctuation is weakened and the fluctuation range is shortened during the pitch line meshing. The analysis of 0(b) indicates that the axial force mainly includes the axial component of the meshing force and axial friction. The normal contact force is the major drive to realize the traction of the shearer, which inevitably increases with the increase in the traction load. The axial friction resistance also increases according to the Coulomb friction theory. And the axial component of the meshing force is the driving force of axial sliding and its direction is the same as the

sliding, and the dynamic friction force is the result of the sliding and its direction is opposite to the sliding. As a result, it can be inferred that the increase of axial force is the common result of the increase of dynamic friction and axial meshing force, and the increase of axial meshing force is greater than that of friction force. This manifests that the axial friction loss on the tooth increases with the increase of traction power when the traction wheel is forced to slide axially affected by the shearer's attitude. Therefore, the wear failure of traction wheels of high-power shearers due to axial sliding cannot be ignored.

With the increase of traction load, axial sliding decreases overall, the maximum sliding speed decreases by 35% to  $1.12 \times 10^{-4}$  m/s and its fluctuation decreases, as shown in 0(b) and (d). Therefore, the longitudinal vibration of the shearer traction units is reduced without external forced driving. And since the alternating stress of the tooth surface decreases with the weakening of the sliding velocity, the destructive effect of the axial sliding near the tooth tip is relatively weakened with the increase of the traction load. This is related to the increase

of axial sliding friction and the change of meshing contact clearance. And with the increase of traction load, the contact deformation of traction wheels and the bearing width increase by the influence of normal load, and the difference in axial stress distribution decreases. This results in the reduction of the contact clearance and the decrease of the axial sliding trend of

the tooth surface. When the dual-drive load of the shearer is unbalanced, the load of one traction unit decreases sharply while the other side increases. Therefore, the load loss of the traction wheels will lead to the aggravation of axial sliding, and the risk increase of axial slip wear on the tooth surface.

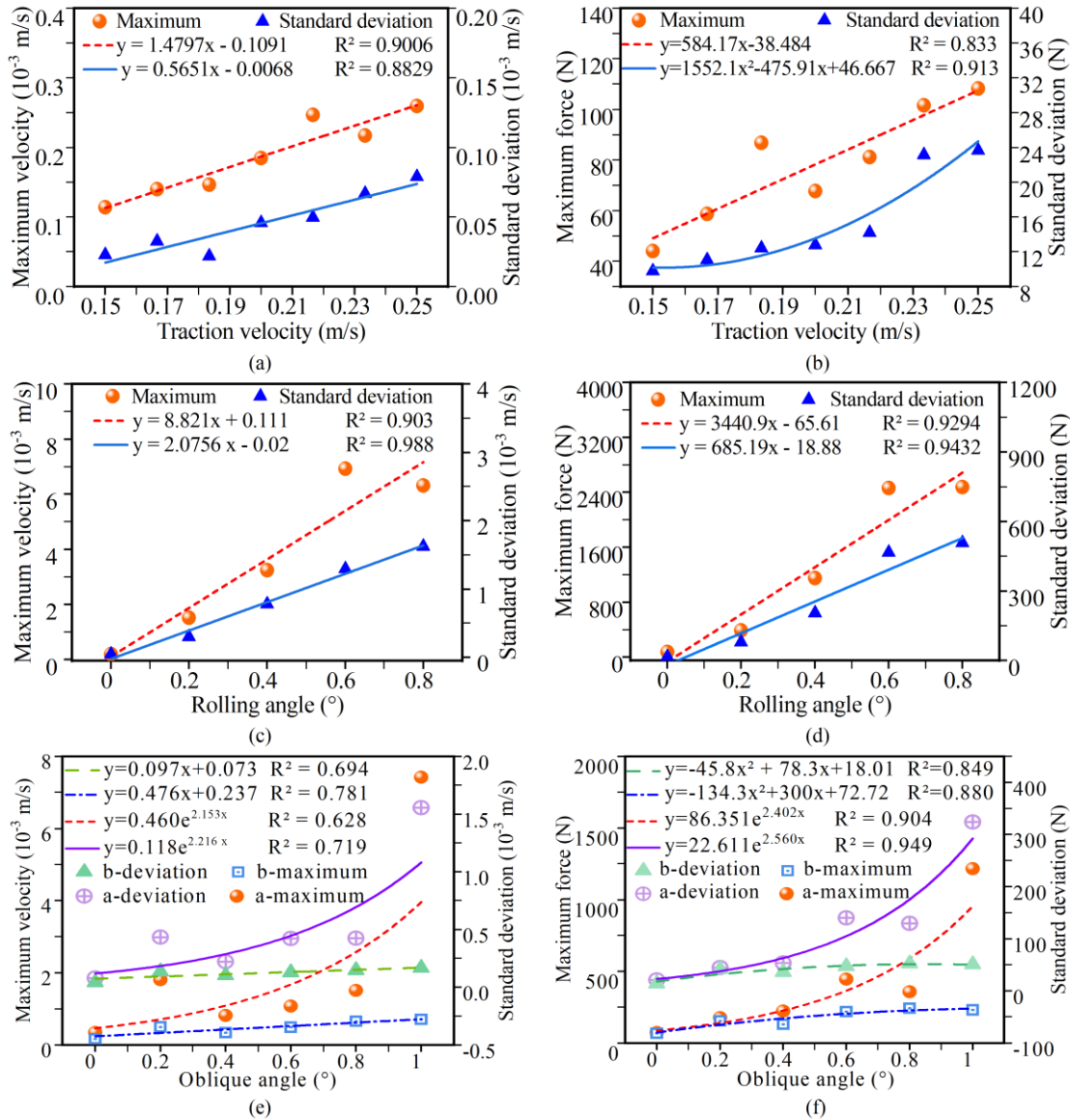


Fig. 11. Axial sliding response of the traction wheel: (a) axial speed affected by the traction speed; (b) axial force affected by the traction speed; (c) axial speed affected by the rolling angle; (d) axial force affected by the rolling angle; (e) axial speed affected by the oblique angle; (f) axial force affected by the oblique angle.

Traction speed is an important factor affecting the meshing contact and tooth friction behavior of traction wheels. Therefore, to explore the response of axial sliding to traction speed, the traction speed is set between 0.15 m/s and 0.25 m/s respectively, and the traction load is 120 kN. According to the above method, the maximum axial sliding speed and axial force when the stable meshing are obtained respectively, as shown in 0(a) and 0(b).

The results show that the maximum axial force and sliding velocity increase, with the increase of hauling velocity, and the fluctuation of sliding force and velocity intensifies. This is because the contact period of a single tooth decreases with the increase of traction speed, and the increase of meshing frequency leads to the axial sliding aggrandize.

In addition, the increase in traction speed leads to the tooth

collision intensification and an increased axial component of meshing impact force. And the normal force on the tooth surface is related to the traction load [53, 54]. When its change is weak, the axial sliding friction coefficient decreases with the increase in sliding speed. The increase of meshing impact force and the decrease of friction force together lead to an increase in the axial force. Furthermore, it may be the reason for the fluctuation increase of axial force and sliding speed that the impact amplitude and frequency of the meshing increase. Therefore, attention should be paid to the friction frequency of the axial sliding of the tooth surface, in the design of high-speed shearers. And the destructive effect of the alternating stress on the tooth should be considered.

Affected by the walking attitude disturbance, there is a tooth surface angle error in the actual meshing between the pin track and traction wheels. Rolling angle  $\theta$  and oblique angle  $\lambda$  of the traction wheel relative to the pin track leads to the difference in the axial stress distribution on the tooth surface, which may be an important factor to induce the axial sliding. Therefore, to explore the influence of the meshing angle error on the axial sliding,  $\theta$  is set as 0 to 0.8°,  $\lambda$  as 0 to 1°, the traction speed as 0.25 m/s and the traction load as 120 kN.

As shown in 0(c) and 0(d), the maximum axial force and sliding speed have a good linear correlation with the  $\theta$ . The fluctuation amplitude of the axial force and sliding speed increases, as the increase of the  $\theta$ . The result shows that the maximum axial displacement is  $1.66 \times 10^{-3}$  mm and the axial force reaches 2.477 kN when  $\theta$  reaches 0.8°. And the response sensitivity of axial sliding to  $\theta$  is significantly higher than that of traction speed and traction load. This is because the extrusion contact of one side tooth profile is aggravated after the traction wheel deflects in the x-axle (traction speed direction), and the axial load on the tooth surface is an uneven distribution. The increase in axial force is mainly related to the axial contact force, which leads to the axial forced displacement of the traction wheel. In addition to the rolling contact along the tooth profile direction, the axial slipping friction of the unilateral tooth surface appears, and the wear risks on the teeth edges are increased. The existing research [55] shows that the coupling effect of the high sliding speed and the high contact pressure is a pivotal reason for the gluing failure and adhesion wear of the tooth surface. Therefore, besides inducing the torsional fracture

failure of the tooth, the influence of the lateral overturning attitude of the shearer on the axial friction and tooth surface wear cannot be ignored. The optimal control of the shearer's attitude is a feasible means to restrain the axial sliding failure of traction wheels.

As shown in 0(e) and 0(f), the maximum axial force and sliding speed of the traction wheel increase with the increase of  $\lambda$ . The results indicate that the axial displacement reaches  $6 \times 10^{-4}$  mm and the maximum axial force is 1.216 kN when  $\lambda$  reaches 1°. However, different from the influence of  $\theta$ , the periodicity of the influence of  $\lambda$  on axial sliding gradually disappears, and the sliding is divided into a-stage (0 to 1.2 s) and b-stage (1.2 s to 2 s). During the period from 0 to 1.2 s (the initial meshing phase with  $\lambda$ ), the axial sliding increases exponentially with the change of  $\lambda$ . At the meshing initial stage, the sensitivity of the axial sliding to the  $\lambda$  increases sharply, and the axial force increases significantly. After 1.2 s (the end meshing phase with  $\lambda$ ), the influence of  $\lambda$  gradually reaches the saturation state and the axial displacement changes slightly. This is because the traction speed produces an axial speed component of the traction wheel affected by the  $\lambda$ . This is the main reason for the aggravation of the axial sliding at the initial meshing phase with  $\lambda$ . The axial sliding gradually tends to be saturated caused by the constraint of the pin track rib plate, as the increase of time, but the eccentric load near the top area on the teeth surface is not improved. And with the increase of  $\lambda$ , the traction wheel may even seriously derailment, and the stress near the tooth surface top exceeds the material yield limit due to the impact contact and structural interference. This indicates that the tooth surface wear caused by the axial sliding induced by the  $\lambda$  is mainly concentrated in the initial meshing phase with  $\lambda$ . Although the axial sliding behavior decreases with time, the meshing collision near the tooth surface top does not improve. Especially when the multi-tooth alternating meshing, the impact failure risk of the tooth surface top increases with the  $\lambda$ . Therefore, the accurate control of the scraper conveyor and the trajectory optimization of the shearer has a positive effect on reducing the oblique meshing error of traction wheels, which is conducive to improving the reliability of traction wheels.



### 3.3. Analysis of the axial forced sliding under the different sliding positions

According to the above discussion, the axial sliding of traction wheels in a single meshing cycle has obvious differences in different tooth profile positions. Besides, existing studies show that the meshing impact is an important cause of tooth surface damage, which is mainly distributed in the meshing-in area, pitch line area and meshing-out area [56, 57]. Furthermore, in the shearer's actual traction, the axial sliding of the traction wheel is forced to intensify due to the interference of the shearer's attitude and the structure of the traction unit. Therefore, to explore the difference in the destructiveness of axial sliding on different tooth profile positions, the axial driving force of 80 N is added near the tooth root, pitch line and tooth top areas to force the axial sliding. The three dangerous areas correspond to the element contact time of the first, fourth and seventh rows on the tooth surface. The generation times of the axial driving force are set as 1.128 s to 1.16 s, 1.396 s to 1.428 s, and 1.652 s to 1.684 s, respectively.

As shown in 0, the hauling force  $F_t$  of traction wheels and the axial contact force  $F_z$  are obtained, respectively. Taking the

second meshing period (1.08 s to 1.82 s) as an example, the fluctuation trend of  $F_t$  is the same under different axial sliding. The maximum  $F_{t1}$  of the second tooth is 132 kN at 1.09 s, in the free sliding state; but it is reduced to 128 kN, 125 kN and 128 kN, respectively, in the axial forced sliding state. This shows that the axial forced sliding can reduce the effective traction capacity of traction wheels. And the traction loss with a decrease of 5% is the most significant when the axial sliding near the pitch line. In addition, different from free sliding,  $F_z$  increases when the tooth surface is forced to axial sliding, and it is the most serious in the meshing-in area. The maximum axial force of the forced sliding is 125 N, 89.3 N and 76.2 N, respectively. And the corresponding time is 1.16 s, 1.41 s and 1.69 s, respectively. This is basically consistent with the setting time of the axial driving force. Therefore, in addition to the axial component of the meshing force, this result reveals that the external axial forced driving force is a key factor affecting axial sliding. The above analysis explains that, during the meshing process from the tooth root to the top, the destructiveness of axial forced sliding is the most serious around the tooth root but weakened near the tooth top.

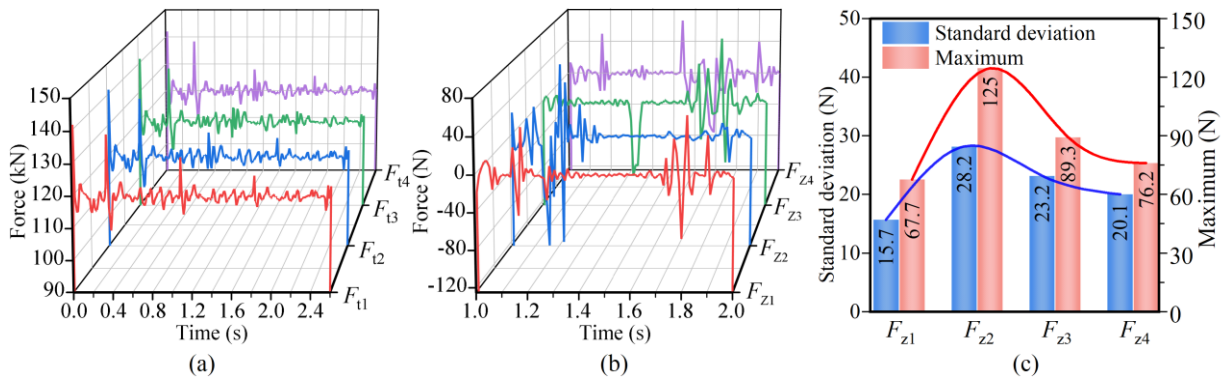


Fig. 12. Axial sliding contact properties of the traction wheel in the various positions:(a) the traction force; (b) axial force; (c) maximum value and variance of the axial force.

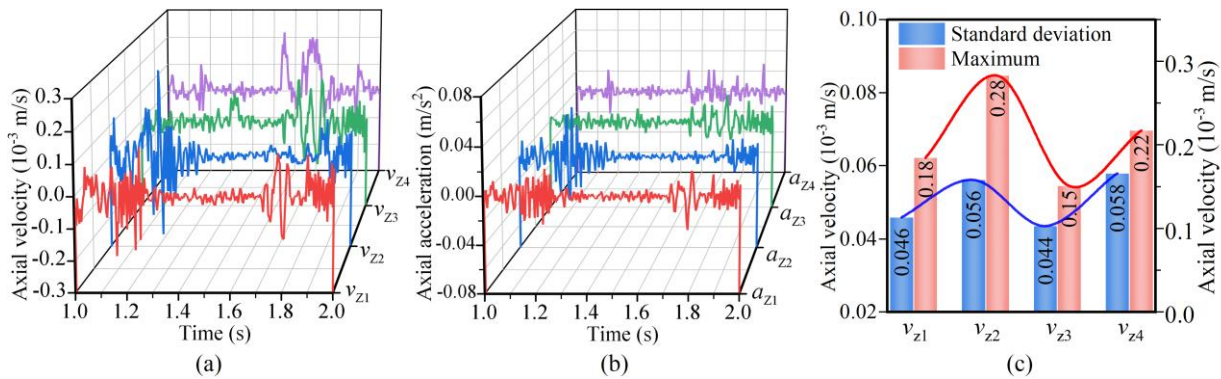


Fig. 13. Axial sliding motion characteristics of the traction wheel at different positions: (a) axial velocity; (b) axial acceleration; (c) maximum value and variance of axial velocity.

As shown in 0, the axial speed  $v_z$  and axial acceleration  $a_z$  of the traction wheel are obtained, respectively. The results show that, compared with the axial free sliding, the  $v_z$  near the tooth root and tip increases significantly during the existence of the axial forced driving force, but  $v_z$  changes slightly near the pitch line. This results in that, nearer the tooth root, axial sliding behavior is more easily induced by the shearer's attitude and the sliding friction frequency increases. Therefore, during the meshing process from the tooth root to the top, the axial sliding behavior and fatigue wear near the tooth root are aggravated under the same external driving force.

Stress analysis is of great significance to reflect the wear and load distribution of the tooth. Therefore, to explore the influence of the sliding position on tooth failure, the maximum stress of the tooth with different sliding forms is obtained, as shown in 0. The results show that the maximum stress is 525 MPa when the

axial forced sliding of the tooth root, 508 MPa of the pitch line and 523 MPa of the tooth top. Compared with free sliding, the stress concentration time on the teeth profile is longer after the axial forced sliding in the tooth root. This reflects that the influence time of the axial sliding around the tooth root is longer while the influence on the tooth profile wear is stronger. Besides, the results show that the stress changes slightly after the axial forced sliding on the pitch line, and the stress concentration at the tooth top is improved. This is related to the reduction of the axial contact force and  $v_z$  (as shown in 0 and 0) when the pitch line area is forced to slide. Furthermore, the stress result shows that the axial eccentric load on the tooth surface increases after the axial forced sliding near the tooth top. This is an important reason for inducing tooth deformation from the constrained torsional.

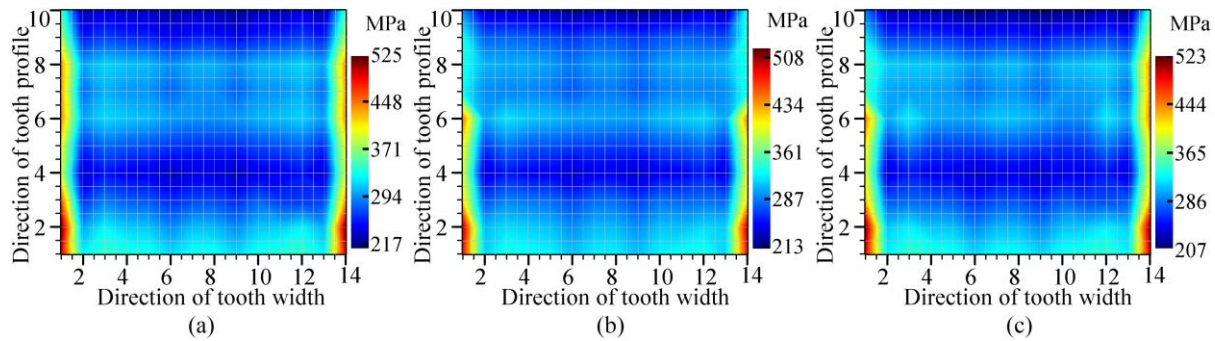


Fig. 14. Maximum stress distribution of the traction wheel under axial forced sliding: (a) sliding near the tooth root; (b) sliding near the pitch line; (c) sliding near the tooth top.

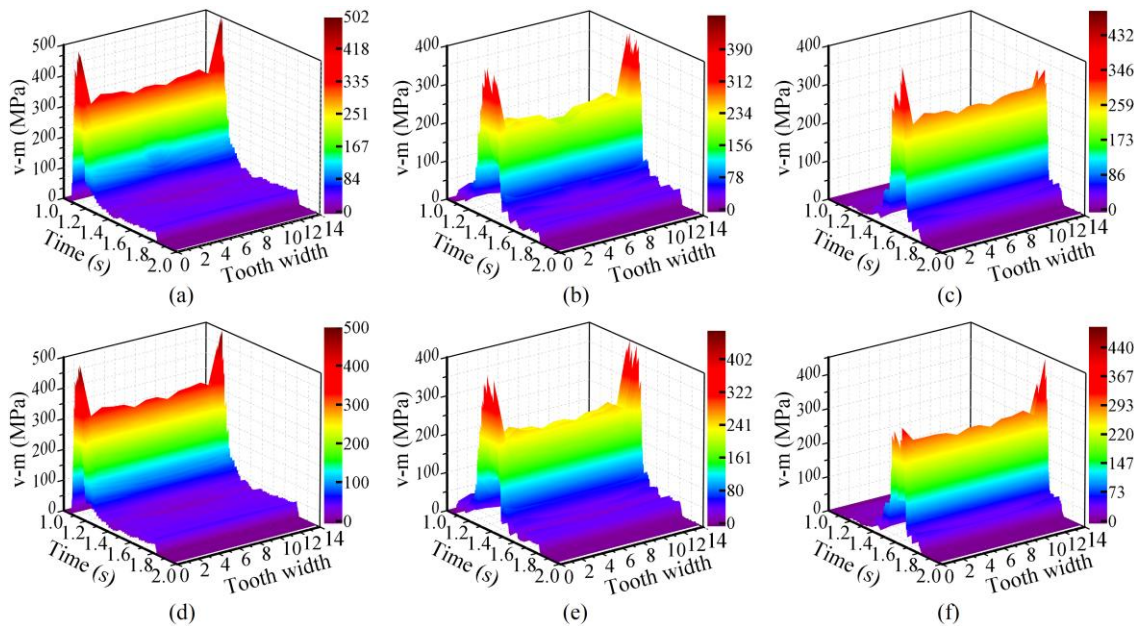
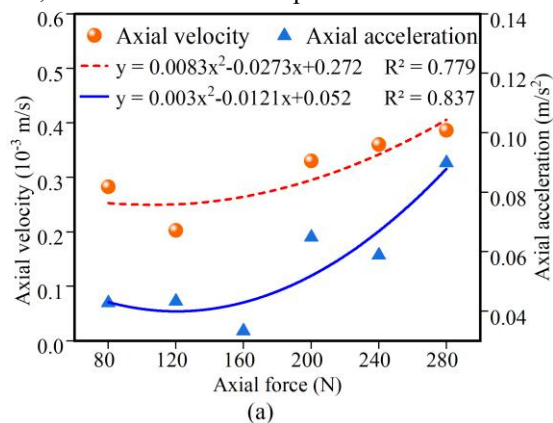


Fig. 15. Stress in different areas on the tooth surface of the traction wheel: (a) tooth root with free sliding; (b) the pitch line with free sliding; (c) tooth top with free sliding; (d) tooth root with forced sliding; (e) the pitch line with forced sliding; (f) tooth root with forced sliding.

To further explore the stress damage difference of the tooth surface near the tooth root, pitch line and tooth tip caused by the axial sliding, the stress states of the elements in the first, fourth and seventh rows are obtained respectively, as illustrated in 0. The result indicates that the tooth surface stress in the three areas under forced sliding is basically the same as that under free sliding, and the stress on the tooth profile changes slightly. When forced sliding, the maximum equivalent stress is 500 MPa around the tooth root, 402 MPa near the pitch line, and 440 MPa around the tooth tip. During the duration of the axial driving force, the stress is basically maintained above 330 MPa around the tooth root, the pitch line area is about 235 MPa, and the tooth tip area is about 290 MPa. This reveals that in the meshing process from the tooth root to the tooth top, the axial sliding driven by the same external force to the tooth root is the most destructive, but the stress near the pitch line and the tooth



top is more sensitive to forced sliding. Combined with the analysis of  $v_z$  and  $F_z$  on the tooth surface, besides the traditional bending fatigue and rolling contact fatigue damage around the tooth root meshing area, the torsional deformation around the traction wheel's radial occurs under the action of axial force and axial friction. Therefore, in the design of the shearer with complex attitude disturbance, the torsional fatigue damage of axial sliding to the traction wheel's root cannot be ignored.

The above analysis reflects that the axial forced sliding and its harm around the tooth root of the traction wheel are obviously more serious than that in other areas. Therefore, to further research the effect of driving force on the axial forced sliding of the tooth surface, only the response of the axial forced sliding near the root area under different driving forces is studied. The axial driving force is set as 80 kN to 280 kN. The  $F_z$ ,  $v_z$  and tooth surface stress are obtained, as shown in 0 and 0.

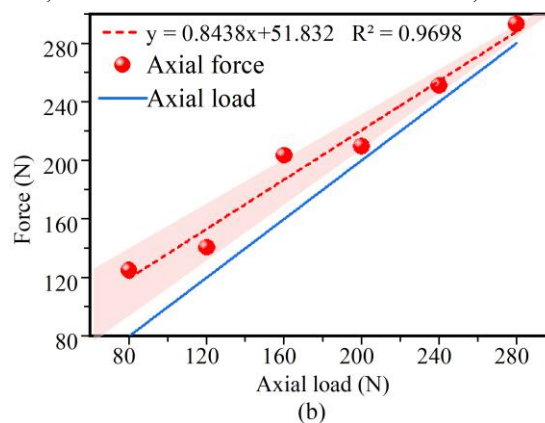


Fig. 16. The influence of axial driving force on axial forced sliding on the tooth surface: (a) axial sliding velocity; (b) axial contact force.

The results show that, with the increase of axial driving force, the  $F_z$  and  $v_z$  increase, and the reciprocating sliding fluctuation intensifies, as shown in 0. As the driving force increases, the response sensitivity of  $v_z$  is higher, the  $v_z$  increases by 36% from  $2.83 \times 10^{-3}$  m/s to  $3.86 \times 10^{-3}$  m/s. This is the inevitable result of increased external incentives. Besides, the  $F_z$  exhibits a near-linear correlation with the driving force during forced sliding, and the correlation increases with the increase of the driving force. This may be because, with the sliding intensifying, the driving force and the meshing force increase in the sliding direction, while the influence of friction is relatively weakened in the opposite direction of the sliding. Therefore, besides the meshing speed, load and meshing angle, the attitude and axial load of the shearer are important reasons causing the axial sliding of the traction wheels.

To characterize the failure risk, the tooth safety factor  $K_s$  is

defined as the ratio of the allowable stress divided by the maximum stress. A smaller safety factor indicates a higher failure risk due to tooth stress. The simulation results show that the load difference is significant on the tooth profile. And combined with the above analysis, the axial stress distribution is uneven under the combined bending and torsion deformation of the tooth. Therefore, the response characteristics of  $K_s$  to the axial driving force are obtained, in the tooth profile area and the middle of the tooth width, respectively. The results show that, under the influence of concentrated stress, the  $K_s$  of the tooth profile is significantly lower than that in the middle of the tooth width, and the  $K_s$  of the tooth profile is more sensitive to the driving force. With the increase of driving force, the  $K_s$  around the tooth root decreases, both in the tooth profile and the tooth middle. This is the inevitable result of the intensification of the axial sliding during the existence of the driving force. And this



reflects that the contact fatigue strength around the tooth root decreases, with the increase of the driving force, and the contact wear risk on the tooth surface increases. Besides, in the single tooth meshing cycle, the tooth top is more affected by the axial driving force, but the response of other areas to the driving force is weakened. This may be because, when the contact position migrates from the tooth root to the tooth tip, the affected area of the tooth bending and torsional deformation is mainly the tooth root. In conclusion, the destructiveness to the tooth surface caused by the increased driving force is mainly around the tooth root but is weak near the pitch line and tooth top.

The differences in tooth surface contact results in uneven axial load distribution. Therefore, to characterize the axial eccentric load on the tooth, the tooth surface stress distribution coefficient  $K_\sigma$  is defined by the ratio of the maximum stress to the minimum stress on the same meshing line. The results show that the eccentric load near the meshing-in area is serious, and

the axial eccentric load in the later period of a meshing cycle increases as the axial driving force increase. The eccentric load leads to the shortening of the effective tooth width and the load increase on the tooth single side, which are important factors inducing unilateral wear and torsional deformation. Therefore, the torsional destruction to the wheel body and the wear damage on the tooth top due to the forced sliding will increase with the increase of the driving force. The axial load of the drum and the axial collision of traction units are the main sources of the driving force of traction wheels. Therefore, it is of positive significance to suppress the damage of axial sliding that optimizing the axial cutting load by changing the operating parameters and the drum structure. And it is a feasible means to improve the useful life of traction wheels that reduces the axial impact force of traction units through the shearer's attitude control.

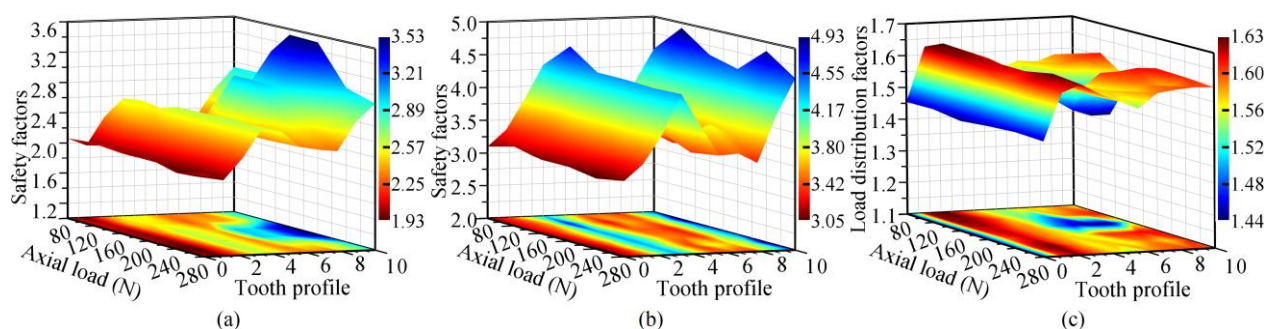


Fig. 17. The influence of axial driving force on tooth surface stress: (a) the safety factor of tooth profile; (b) the safety factor in the middle of the tooth width; (c) stress distribution coefficient on the tooth surface.

#### 4. Conclusions

To reveal the failure laws on the traction wheels caused by axial sliding, a meshing contact model between the pin tracks and the traction wheel with axial sliding is established. The differences in meshing contact of the tooth surface are compared. The response laws of the axial sliding to the traction load, traction speed, and meshing angle are analyzed. And the influences of the sliding position and driving strength on the tooth meshing and failure with axial forced sliding are discussed. The following conclusions are made:

1) The axial sliding predominantly occurs during the multi-tooth alternating meshing stage, and the sliding is relatively weakened near the pitch line. It demonstrates dual mechanical effects: a reduction of more than 50% in axial impact forces at tooth-profile interfaces and a mitigating of the eccentric loading

around the tooth top; a stress increase of 52 MPa on the tooth surface near the tooth root and a risk increase of brittle fracture.

2) With the increase of traction load from 80 kN to 160 kN, the axial friction on the tooth surface increases but the sliding speed near the tooth top decreases by 35% to  $1.12 \times 10^{-4}$  m/s. Traction speed, rolling angle and oblique angle promote the tooth axial sliding behavior, which leads to an increase in adhesion wear and gluing failure. And the response of sliding to the rolling angle is the most significant.

3) When the rolling angle reaches  $0.8^\circ$ , the maximum axial displacement is  $1.66 \times 10^{-3}$  mm, and the unilateral tooth profile wear is aggravated due to the tooth eccentric load. The tooth surface wear induced by the oblique angle is mainly concentrated in the initial stage of the oblique angle. With the advance of time, the sliding behavior decreases but the failure risk of impact contact near the tooth top increases sharply.



Therefore, the attitude optimization of the shearers is a feasible means to suppress the axial sliding failure of traction wheels.

4) Axial forced sliding reduces the effective traction capacity of the shearer, and traction force near the pitch line reduces by 5% with a driving force of 80 N. Compared with the areas near the pitch line and tooth top, the axial driving force is more likely to induce the sliding behavior near the tooth root. As the driving force increases from 80 N to 280 N, the axial forced sliding increases by 36% from  $2.83 \times 10^{-3}$  m/s to  $3.86 \times 10^{-3}$

m/s and the contact strength near tooth root decreases, the wear damage near the tooth top and the torsional deformation on the tooth intensify.

The results have a reference for reducing the traction failure of shearers. The load distribution between the double traction units has an important influence on the dynamic characteristics of the traction wheel. Therefore, the axial sliding response analysis under the load synergistic coupling between the dual traction units can be considered in future research.

## Acknowledgments

This research was funded by China Postdoctoral Science Foundation (GZC20240948; 2025M771785); the Shandong Postdoctoral Science Foundation (SDCX-ZG-202400230); the National Natural Science Foundation of China (52504167; U23A20599; 52474175; 52474176). Thank you to Dr. Kao Jiang and Prof. Kuidong Gao for their help.

## References

1. Wang D, Xu Y, Zhang B, et al (2024) Numerical simulation of low-rank coal drying based on non-equilibrium thermodynamics. *Int J Coal Prep Util*. <https://doi.org/10.1080/19392699.2024.2432580>
2. Korsi J (2021) Longwall shearer haulage systems - a historical review. Part 2 – First cordless haulage systems solutions. *Min Mach* 39:24–33. <https://doi.org/10.32056/KOMAG2021.2.3>
3. Zhang P, He Y, Ma L, Cong C (2024) A storm frame optimization method for predicting and warning the safety status of a shearer. *Energy Science & Engineering*. <https://doi.org/10.1002/ese3.1953>
4. Wan L, Wang J, Ma D, Zeng Q (2024) Thermo-mechanical coupling characteristics of the shearer's guiding shoe during the friction. *Sci Rep* 14:24825. <https://doi.org/10.1038/s41598-024-76505-8>
5. Wang S, Wang S (2020) Improving the shearer positioning accuracy using the shearer motion constraints in longwall panels. *IEEE Access* 8:52466–52474. <https://doi.org/10.1109/ACCESS.2020.2980677>
6. Ma D, Zhang X, Wan L, et al (2020) Dynamic analysis of shearer traction unit considering the longitudinal swing. *Energies* 13:5293. <https://doi.org/10.3390/en13205293>
7. Liu C, Qin D, Liao Y (2017) Electromechanical dynamic analysis for the cutting transmission system of the unmanned long-wall shearer under variable speed process. *J Vibroengineering* 19:3191–3206. <https://doi.org/10.21595/jve.2017.17724>
8. Liu C, Yin X, Liao Y, et al (2020) Hybrid dynamic modeling and analysis of the electric vehicle planetary gear system. *Mech Mach Theory* 150:103860. <https://doi.org/10.1016/j.mechmachtheory.2020.103860>
9. Lao J, Wang X, Zhang M, et al (2025) Analysis and improvement of coal-loading performance and reliability of thin seam coal shearer drums. *Eksplot Niezawodn - Maint Reliab* 27:194674. <https://doi.org/10.17531/ein/194674>
10. Yang X, Zou X, Zhang S, et al (2021) Dynamical behavior of coal shearer under the influence of multiple factors in slant-cutting conditions. *Sci Rep* 11:18447. <https://doi.org/10.1038/s41598-021-98049-x>
11. Cheng X, Yang H, An L (2019) Strength analysis and tooth shape optimization design of the pin rail wheel of the shearer. *Mach Tool & Hydraul* 47:114–120. <https://doi.org/10.3969/j.issn.1001-3881.2019.06.020>
12. Kotwica K, Stopka G, Kalita M, et al (2021) Impact of geometry of toothed segments of the innovative KOMTRACK longwall shearer haulage system on load and slip during the travel of a track wheel. *Energies* 14:2720. <https://doi.org/10.3390/en14092720>
13. Wilk-Kolodziejczyk D, Pirowski Z, Grudzie-Rakoczy M, et al (2021) Selection of materials and development of technology for the production of elements used in conditions of extreme tribological wear. *Arch Foundry Eng* 21:47–54. <https://doi.org/10.24425/afe.2021.138678>
14. He L, Gao J, Leng J, et al (2024) Disassembly sequence planning of equipment decommissioning for industry 5.0: Prospects and Retrospects. *Adv Eng Inf* 62:102939. <https://doi.org/10.1016/j.aei.2024.102939>

15. He L, Pan R, Wang Y, et al (2024) A case study of accident analysis and prevention for coal mining transportation system based on fta-bn-pha in the context of smart mining process. *Mathematics* 12:1109. <https://doi.org/10.3390/math12071109>
16. Gao T (2022) Failure analysis and improvement measures of traction chain wheel of high-power shearer. *Coal Sci Technol* 50:323–326
17. Sun R, Song C, Zhu C, et al (2021) Computational study of pitting defect influence on mesh stiffness for straight beveloid gear. *Eng Fail Anal* 119:104971. <https://doi.org/10.1016/j.engfailanal.2020.104971>
18. Wang X, Yang Y, Wang W, Chi W (2020) Simulating coupling behavior of spur gear meshing and fatigue crack propagation in tooth root. *Int J Fatigue* 134:105381. <https://doi.org/10.1016/j.ijfatigue.2019.105381>
19. Dogan O, Yuce C, Karpat F (2021) Effects of rim thickness and drive side pressure angle on gear tooth root stress and fatigue crack propagation life. *Eng Fail Anal* 122:105260. <https://doi.org/10.1016/j.engfailanal.2021.105260>
20. Vučković K, Čular I, Mašović R, et al (2021) Numerical model for bending fatigue life estimation of carburized spur gears with consideration of the adjacent tooth effect. *Int J Fatigue* 153:106515. <https://doi.org/10.1016/j.ijfatigue.2021.106515>
21. Blais P, Toubal L (2021) Fatigue of short-natural-fiber-reinforced high-density polyethylene: Stochastic modeling of single-gear-tooth bending. *Fatigue Fract Eng Mater Struct* 44:1241–1256. <https://doi.org/10.1111/ffe.13426>
22. Li C (2017) Research on time-variant wear reliability of gear rack. *Int J Mech Eng Appl* 5:112. <https://doi.org/10.11648/j.ijmea.20170502.16>
23. Jafari A, Nezhad VS (2016) Employing DEM to study the impact of different parameters on the screening efficiency and mesh wear. *Powder Technol* 297:126–143. <https://doi.org/10.1016/j.powtec.2016.04.008>
24. Jafari A, Abbasi Hattani R (2020) Investigation of parameters influencing erosive wear using DEM. *Friction* 8:136–150. <https://doi.org/10.1007/s40544-018-0252-4>
25. Dimaki A, Dudkin I, Popov V, Shilko E (2019) Influence of the adhesion force and strain hardening coefficient of the material on the rate of adhesive wear in a dry tangential frictional contact. *Russ Phys J* 62:1398–1408. <https://doi.org/10.1007/s11182-019-01857-y>
26. Huang S, Li B, Ma H, et al (2025) Design and evaluation of abrasive wear testing device for scraper conveyor middle plates. *Powder Technol* 460:121042. <https://doi.org/10.1016/j.powtec.2025.121042>
27. Chen Z, Ji P (2020) Study on wear in spur gears based on an improved load distribution model considering the effects of corner contact. *Eng Fail Anal* 115:104605. <https://doi.org/10.1016/j.engfailanal.2020.104605>
28. Zhang H, Shen X (2020) A dynamic tooth wear prediction model for reflecting “two-sides” coupling relation between tooth wear accumulation and load sharing behavior in compound planetary gear set. *Proc Inst Mech Eng, Part C* 234:1746–1763. <https://doi.org/10.1177/0954406219900085>
29. Zhang X, Yao G, Zhang Y (2021) Nonlinear multi body dynamic modeling and vibration analysis of a double drum coal shearer. *J Cent South Univ* 28:2120–2130. <https://doi.org/10.1007/s11771-021-4757-z>
30. Zhang X (2021) Design and implementation of virtual cooperative operation system of shearer and scraper conveyor under complex floor conditions. Master, Taiyuan University of Technology
31. Wang X, Xie J, Li S (2022) Virtual reality technology in mining machinery. Springer, Singapore. <https://doi.org/10.1007/978-981-16-4408-5>
32. Zhou Y, Zhu C, Liu H, et al (2021) Investigation on stress microcycles and mild wear mechanism in gear contact fatigue. *Fatigue Fract Eng Mater Struct* 44:2265–2279. <https://doi.org/10.1111/ffe.13486>
33. Luo W, Qiao B, Shen Z, et al (2021) Investigation on the influence of spalling defects on the dynamic performance of planetary gear sets with sliding friction. *Tribol Int* 154:106639. <https://doi.org/10.1016/j.triboint.2020.106639>
34. Su Y, Yao L, Zhang J (2021) Contact dynamics analysis of nutation drive with double circular-arc spiral bevel gear based on mathematical modeling and numerical simulation. *Mech Sci* 12:185–192. <https://doi.org/10.5194/ms-12-185-2021>
35. Zhao B, Huangfu Y, Ma H, et al (2020) The influence of the geometric eccentricity on the dynamic behaviors of helical gear systems. *Eng Fail Anal* 118:104907. <https://doi.org/10.1016/j.engfailanal.2020.104907>
36. Che X, Zhang C, Yu H, Zhu R (2025) The investigation of nonlinear dynamic characteristics of spur gear with angular misalignment error based on an improved dynamic model. *Commun Nonlinear Sci Numer Simul* 141:108476. <https://doi.org/10.1016/j.cnsns.2024.108476>
37. Liu N, Ma H, Zhao Z, et al (2024) Dynamic characteristics of gear-rotor system with gear eccentricity and wear fault. *Nonlinear Dyn*

112:16003–16035. <https://doi.org/10.1007/s11071-024-09879-z>

38. Wan Q, Chen J, Chen W, Zhu R (2024) An effective method for identifying uneven load distribution on the tooth faces of misaligned wide-faced helical gear pairs. *IEEE Sens J* 24:36569–36578. <https://doi.org/10.1109/JSEN.2024.3472024>
39. Dong J, Tang J, Hu Z (2021) Dynamic characteristics of the face gear transmission system based on a rotor-shaft-bearing model with multiple nodes. *Int J Non-Linear Mech* 137:103825. <https://doi.org/10.1016/j.ijnonlinmec.2021.103825>
40. Lu S, Ding H, Rong K, et al (2022) Composite mechanical deformation based semi-analytical prediction model for dynamic loaded contact pressure of thin-walled aerospace spiral bevel gears. *Thin-Walled Struct* 171:108794. <https://doi.org/10.1016/j.tws.2021.108794>
41. Mo S, Ma S, Jin G (2019) Research on composite bending stress of asymmetric gear in consideration of friction. *Proc Inst Mech Eng Part C-J Eng Mech Eng Sci* 233:2939–2955. <https://doi.org/10.1177/0954406218797975>
42. Ma D, Wan L, Lu Z, et al (2021) Research on the traction dynamic of shearer based on the pose analysis. *Eng Fail Anal* 130:105760. <https://doi.org/10.1016/j.engfailanal.2021.105760>
43. Zhao Y (2019) Numerical Simulation Study on Wear Failure of Spiral Drum in Gangue-containing Coal Seam. Master, Liaoning Technical University
44. Wan L, Ma D, Zhang X (2020) Research on meshing characteristics of shearer walking wheel based on rigid-flexible coupling. *Math Probl Eng* 2020:8301086. <https://doi.org/10.1155/2020/8301086>
45. Ma D, Wan L, Zhang X, et al (2022) Meshing characteristics and failure analysis of shearer walking wheel considering torsional deformation. *Alex Eng J* 61:5771–5782. <https://doi.org/10.1016/j.aej.2021.09.035>
46. Chen R, Zhang J, Zhou Jianxing, Sun W (2016) Study on the meshing stiffness of spur gear considering contact characteristic of tooth surface. *J Mech Transm* 40:43–47+53. <https://doi.org/10.16578/j.issn.1004.2539.2016.10.009>
47. Hu Y, Du Q, Xie S (2023) Nonlinear dynamic modeling and analysis of spur gears considering uncertain interval shaft misalignment with multiple degrees of freedom. *Mech Syst Signal Proc* 193:110261. <https://doi.org/10.1016/j.ymssp.2023.110261>
48. Bai Y (2020) Study on the dynamic characteristics of stick-slip friction in the walking unit of shearer. Doctor, Liaoning Technical University
49. Ma D, Wan L, Gao K, et al (2022) The meshing and failure analysis of haulage wheels with the effect by shearer's poses. *Eng Fail Anal* 137:106251. <https://doi.org/10.1016/j.engfailanal.2022.106251>
50. Chen R, Zhang J, Zhou J, Sun W (2017) A study on the dynamic characteristics of a planetary gear system with considering contact tooth surface. *J Vib Shock* 36:180–187. <https://doi.org/10.13465/j.cnki.jvs.2017.20.028>
51. Osman T, Velez Ph (2010) Static and dynamic simulations of mild abrasive wear in wide-faced solid spur and helical gears. *Mech Mach Theory* 45:911–924. <https://doi.org/10.1016/j.mechmachtheory.2010.01.003>
52. Xiujian T, Wang L, Yang N, et al (2021) Experimental study on friction and wear of ground surface of 20CrMnTi steel gear. *Tool Eng* 55:69–72. <https://doi.org/10.3969/j.issn.1000-7008.2021.04.015>
53. Tamai Y, Inazumi T, Manabe K (2016) FE forming analysis with nonlinear friction coefficient model considering contact pressure, sliding velocity and sliding length. *J Mater Process Technol* 227:161–168. <https://doi.org/10.1016/j.jmatprotec.2015.08.023>
54. Voyiadjis GZ, Deliktas B, Faghihi D, Lodygowski A (2010) Friction coefficient evaluation using physically based viscoplasticity model at the contact region during high velocity sliding. *Acta Mech* 213:39–52. <https://doi.org/10.1007/s00707-010-0294-9>
55. Morales-Espejel GE, Gabelli A (2019) Rolling bearing seizure and sliding effects on fatigue life. *Proc Inst Mech Eng Part J-J Eng Tribol* 233:339–354. <https://doi.org/10.1177/1350650118779174>
56. Ding H, Rong S, Rong K, Tang J (2022) Sensitive misalignment-based dynamic loaded meshing impact diagnosis mechanism for aviation spiral bevel gear transmission. *Expert Syst Appl* 200:116969. <https://doi.org/10.1016/j.eswa.2022.116969>
57. Zhou C, Tang J, Zhong Z (2008) Corner contact and impact friction of gear drive. *J Mech Eng* 44:75–81. <https://doi.org/10.3901/JME.2008.03.075>